European Journal of Medicinal Chemistry Reports 11 (2024) 100157

Contents lists available at ScienceDirect

European Journal of Medicinal Chemistry Reports

journal homepage: www.editorialmanager.com/ejmcr/default.aspx

A novel approach toward the multigram synthesis of a novel Bcl2-specific inhibitor, and evaluation of its biological activity

Manthra Raveendran [a], Shivangi Sharma [a], Sanjay Sambhajirao Palimkar [b], M. Lakshmana Kumar [b], H. Sahana [b], Hassan A. Swarup [a,c,**], Sathees C. Raghavan [a,*]

[a] Department of Biochemistry, Indian Institute of Science, Bangalore, 560012, India
[b] Department of Process Chemistry, Eurofins Advinus Biopharma Services India Pvt. Ltd. Phase II, Peenya Industrial Area, Bangalore, 560058, India
[c] Department of Chemistry, B N M Institute of Technology, Bangalore, 560070, India

ARTICLE INFO

Keywords:
BCL2 inhibitor
Apoptosis
Cancer therapy
imidazo[2,1-b][1,3,4]thiadiazole-linked oxindole
Domino reaction
Targeted therapy

ABSTRACT

The antiapoptotic protein BCL2 is overexpressed in several cancers. It contributes to prolonged cell survival and chemoresistance, making it an excellent target for targeted cancer therapy. Over the years, several BCL2 inhibitors have been investigated extensively for their anticancer potential; however, most of them were abolished before clinical use due to their pan activity. There is only one FDA-approved BCL2-specific inhibitor, Venetoclax, currently used in clinics. Previously, we reported the characterization and development of a novel BCL2 inhibitor, Disarib, which is selective against BCL2 and predominantly binds to the BH1 domain of BCL2. Importantly, the efficacy of Disarib was equally good or better than Venetoclax in various *in vitro* and *in vivo* assays. In the present study, we report the development of a scalable and practical method for the large-scale synthesis of Disarib to support the ongoing pre-clinical studies. The parameters of each step were optimized through prior knowledge, helping in improving the yield and purity to 98.8 %. Further, we compared the efficiency of a large-scale synthesized Disarib in a GLP-certified laboratory with that of an in-house synthesized Disarib. The results showed that the biological activity, including Disarib-induced cytotoxicity and cell cycle progression, were comparable. Besides, the tumor regression efficacy and pharmacokinetics analysis of Disarib have shown comparable results when Disarib synthesized in both routes were tested. Thus, a robust and scalable synthetic pathway of Disarib has developed to address small-scale synthesis's limitations in supporting their expanded applications and use.

1. Introduction

Apoptosis, or programmed cell death, is a regulatory process that plays a prime role in the development and maintenance of homeostasis [10,15]. One of the hallmarks of cancer cells is the deregulation of apoptosis. BCL2 family proteins are key players in the process of apoptosis, which regulates the apoptosis via interactions of pro and antiapoptotic members of the family [30,42].

BCL2, one of the first antiapoptotic genes associated with apoptosis, regulates the intrinsic pathway of apoptosis and is involved in the complex network of protein-protein interactions between antiapoptotic (BCL2, BCL-xL, BCL2A1, BCLw, and MCL1) and proapoptotic (BAX, BAK, BID, PUMA, BAD and BIM) proteins [15,34]. The homodimerization of proapoptotic proteins results in the formation of pores in the mitochondrial membrane, which permeabilize and depolarize the organelle, thus releasing the cytochrome C and activating caspases that execute the process of apoptosis [5,34].

BCL2 is highly expressed in several cancers, especially in hematological malignancies [15,29]. The upregulation of BCL2 has been reported in leukemias and B-cell lymphomas (60–80 %) and in several additional cancers [3,20,24]. The overexpression of BCL2 provides prolonged survival of cancer cells and chemoresistance [15,33]. Besides, the sensitivity of BCL2 overexpressing cells towards cell death upon their inhibition, even in the presence of other antiapoptotic proteins [21] unfolded the therapeutic strategies targeting BCL2 as a promising treatment modality. For several decades, various strategies have been used to target BCL2 in cancer therapeutics as it lends itself to an excellent target for cancer therapy [9,52].

* Corresponding author.
** Corresponding author. Department of Chemistry, B N M Institute of Technology, Bengaluru, 560070, India.
E-mail addresses: swarupha@yahoo.co.in (H.A. Swarup), sathees@iisc.ac.in (S.C. Raghavan).

https://doi.org/10.1016/j.ejmcr.2024.100157
Received 17 December 2023; Received in revised form 3 April 2024; Accepted 6 April 2024
Available online 10 April 2024

Structure-based in-silico analysis and therapeutic approaches are the key strategies chosen for the development of small molecule inhibitors that can block/target pro-survival BCL2 proteins [11,16,46]. Previously reported BCL2 inhibitors include BCL2 antisense oligonucleotides [14], BH3-derived peptides [37,53] and BH3-targeted small molecule inhibitors [1]. The flexibility in design, and development, offered prominence to small-molecule inhibitors, such as YC137, ABT263 (navitoclax), AT101 (−)-gossypol), and obatoclax (GX15-070) [26,32,43,55]. Several orally active BCL2 inhibitors, such as ABT263, have been studied previously for their flexibility in dosing regimens and ease of dose administration [4,27,52]. Some of these small molecule inhibitors, ABT263, AT101, and GX15-070, were under clinical trials for multiple cancers [25]. The lack of specificity and having other cellular targets were some of the limiting factors faced during the development of these BCL2 inhibitors. Some of the discovered BCL2 inhibitors, such as obatoclax and AT101, turned out to be pan-BCL2 family inhibitors with much lower affinities [52]. These molecules were more toxic to normal cells as they were also interacting with other members of the anti-apoptotic BCL2 family proteins [15,25,52].

So far, only one BCL2-specific inhibitor, Venetoclax (ABT199), has been approved by the FDA for use against acute myeloid leukemia (AML) and chronic lymphocytic leukemia (CLL) [43]. The selective inhibitor of BCL2 and BCL-xL, Navitoclax, was re-engineered to create the potent BCL2 inhibitor Venetoclax through a structure-based reverse engineering process, which showed regression of BCL2 dependant tumors *in vivo* [21]. ABT199 was used as a single agent or in combination for treating hematological malignancies [7], and it operates through the mitochondrial (intrinsic) pathway of apoptosis in a BCL2-dependent manner.

The success history of Venetoclax suggests that targeting specific BCL2 proteins can be a powerful strategy to kill cancer cells. More recently, many BCL2, MCL1, and BCL-xL inhibitors have been developed and are currently under clinical trials [10,12,14,29,30]. However, there are several reports on the resistance caused by the treatment of Venetoclax in patients with multiple hematological malignancies [28]. Venetoclax treatment leads to upregulating MCL1 and BCL-xL and multiple non-recurring BCL2 mutations that block Venetoclax binding [34].

A specific BCL2 inhibitor, Disarib, that predominantly binds to the BH1 domain of BCL2 was discovered in 2015 [15]. The biochemical, biophysical, and *in silico* studies using Disarib demonstrated the strong affinity of Disarib to BCL2, but not to other antiapoptotic BCL2 family members [15,49]. Disarib showed an antitumor effect against multiple tumor models [49] and is currently under pre-clinical trials. Besides, it showed selective sensitivity towards BCL2 overexpressing cancer cells, both *ex vivo* and *in vivo* [15]. The head-to-head comparison of Disarib with the only FDA-approved drug Venetoclax suggests the better efficacy of Disarib than Venetoclax [15,49,50], The acute toxicity analysis of Disarib in two non-rodent species, Swiss albino mice and Wistar rats, revealed that even a dose as high as 2000 mg/kg (limiting concentration) did not cause significant toxicity in mice and rats [40,41]. There was no significant change in blood parameters or kidney and liver functions following the administration of Disarib. Histopathological analysis of different tissues from the treated group revealed normal architecture with no observable cellular damage [40,41]. Thus, the preliminary toxicological profile of Disarib reveals no significant side effects when Disarib was administered orally to mice and rats [40,41]. Hence, Disarib has emerged as a potential BCL2-specific inhibitor with significant tumor regression efficacy and minimal side effects.

The small-scale synthesis of therapeutically important candidates always meets with limited applications, although it is sufficient for initial investigation. When the studies need to expand to take forward the preliminary observations of a potential therapeutic candidate to in-depth *in vivo* investigations and other therapeutic analyses, a sufficient supply of the compound of interest is a limiting factor in several instances [6].

Previously, we have reported the in-house small-scale synthesis of Disarib (Disarib Ss) [15,18], which supported the initial profiling studies. Some of the difficulties during the in-house synthesis were the lower yields, less purity, and the process complexity. Therefore, taking care of these aspects was important for the extensive profiling and evaluation of preclinical candidate Disarib as a potential therapeutic drug molecule. The excellent toxicological profile of Disarib in the preliminary studies encouraged the development of a scalable synthesis method for Disarib that supports the pre-clinical studies. Here, we have developed a scalable synthesis process for Disarib (Disarib Ss) by taking care of the challenges in a large-scale synthesis, which was cost-effective and better efficient, and was conducted in a GLP-certified laboratory. The newly developed method resulted in a synthetic route for multi-kilogram amounts of Disarib with 98.8 % purity and 86.8 % yield. Disarib, synthesized through small-scale and large-scale synthetic routes exhibited comparable biological activity. Thus, the present study describes a new, cost-effective, and robust scalable pathway for the synthesis of Disarib that could support the pre-clinical studies.

2. Results and discussion

In the present study, we designed and developed a scalable synthetic process to generate a multigram quantity of Disarib, the BCL2-specific inhibitor. The Disarib synthesized with enhanced quality and yield can support preclinical toxicological studies. Insufficient supply of drug candidates in the field of clinical evaluation of anticancer agents has always been a drawback in the developmental process. Lower yields, process complexity, etc., were some of the limiting factors faced during the small-scale synthesis of Disarib Ss using the initial synthetic route (Scheme 1) [15] and were less suitable for facile synthesis of Disarib. Thus, herein, we describe the development of a robust and scalable process for the synthesis of BCL2 inhibitor Disarib that resulted in a yield of 86.8 % and 98.8 % purity. This resulted in reducing the overall higher cycle time by combining steps 2 and 3 in Scheme 1 as a single flux domino reaction (Scheme 2) with better yield as compared to the initial synthetic route.

Scheme 1. Initial Synthesis of Disarib **8**.

2.1. Small-scale synthesis of Disarib Ss through initial synthetic route (Scheme 1)

In the initial synthetic route (Scheme 1) 5-(4-chlorobenzyl)-1,3,4-thiadiazol-2-amine **(3)** was prepared from 2-(4-chlorophenyl)acetic acid (17 g, 0.1 mol) **(1)** thiosemicarbazide (13.6 g, 0.15 mol) **(2)** using H_2SO_4 at 70 °C for 7 h [8,15]. After the completion of the reaction, the resulting reaction mixture was quenched with water; the precipitate was filtered, pressed, suspended in water, and neutralized to pH 7.0 with cold aqueous solution of sodium carbonate. The solid chemical was separated by filtration, washed with water, dried, and recrystallized with ethanol. The yield, in this case, was 60 % (13.4 g). In the next step, 6-(4-bromophenyl)-2-(4-chlorobenzyl)imidazo[2,1-b] [1,3,4]thiadiazole **(5)** was synthesized by the condensation of 5-(4-chlorobenzyl)-1,3,4-thiadiazol-2-amine (7 g, 30 mmol) **(3)** with 4-bromophenacyl bromide (8.6 g, 30 mmol) **(4).** The mixture was refluxed in ethanol for 8–10 h [18,22], and after the completion of the reaction, the excess solvent was removed under reduced pressure, and the solid hydrobromide salt was separated, filtered, washed with cold ethanol, and dried. Neutralization of hydrobromide salts with cold aqueous solution of sodium carbonate yielded the corresponding free base, which was filtered and recrystallized with ethanol to yield products, 55 % (6.9 g). Further, a formylation reaction was performed for 6-(4-bromophenyl)-2-(4-chlorobenzyl)imidazo[2,1-b] [1,3,4]thiadiazole (1 g, 4 mmol) **(5)** by standard Vilsmeier-Haack reaction condition using DMF (10 ml) and $POCl_3$ (2.3 g, 15 mmol). In this step, Vilsmeier reagent was added slowly at 0–5 °C while stirring and cooling were maintained for 2 h. Further stirring was continued for 6 h at 80–90 °C [15]. After the completion of the reaction, the resulting

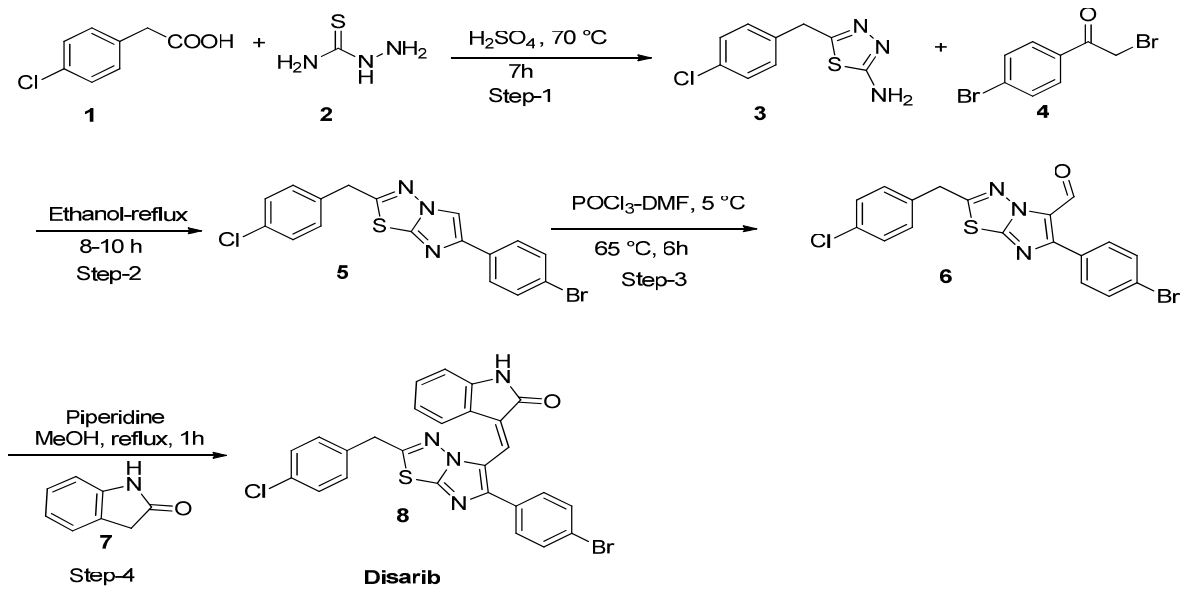

Scheme 1. The initial discovery route for the synthesis of Disarib **(8)**.

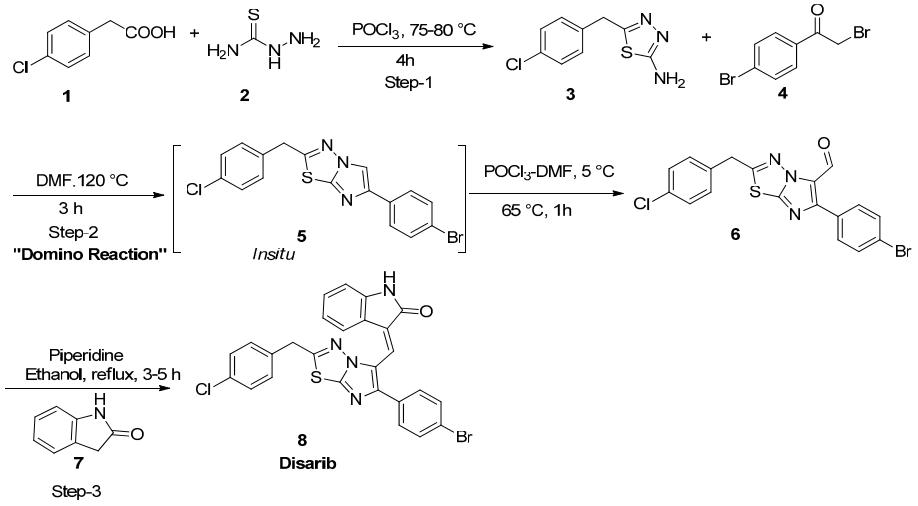

Scheme 2. Scalable synthesis of Disarib **8** after process improvement.

reaction mixture was poured into water, the precipitate was filtered, pressed, suspended in water, and neutralized to pH 7 with cold aqueous solution of sodium carbonate. The solid was separated by filtration, washed with water, dried and crystallized from ethanol to obtain 6-(4-bromophenyl)-2-(4-chlorobenzyl)imidazo[2,1-b] [1,3,4]thiadiazole-5-carbaldehyde **(6)** (48 % yield, 1.2 g).

In the final step, 2-indolinone (1.4 g, 10 mmol) was dissolved in methanol (100 ml) and treated with 6-(4-bromophenyl)-2-(4-chlorobenzyl)imidazo[2,1-b] [1,3,4]thiadiazole-5-carbaldehyde (4.32 g, 10 mmol) **(6)** and piperidine (1 ml). The reaction mixture was refluxed for 1–5 h (the progress of the reaction was monitored by TLC). After the completion of the reaction, the reaction mass was cooled and concentrated under reduced pressure. The resulting precipitate was collected by filtration, and it was purified by recrystallization from ethanol to get pure3-((6-(4-bromophenyl)-2-(4-chlorobenzyl)imidazo[2,1-b] [1,3,4] thiadiazol-5-yl)methylene)indolin-2-one **(8),** Disarib with 85 % yield (4.6 g).

Since the above-mentioned initial route of synthesis (Scheme 1) had drawbacks like obtaining lower yields in the step-1, step-2 and in step-3, and overall higher cycle time, it was not suitable for higher scale synthesis of Disarib. The HPLC analysis of Disarib (8) (Scheme 1) has shown a purity of 91.6 % with 85 % yield. Besides, the evaluation of Disarib as a potential preclinical candidate demanded its higher-scale synthesis, which should be cost-effective and practical. To overcome the drawbacks of the small-scale synthetic pathway (Scheme 1), a robust, scale-up friendly, telescopic, and cost-effective process for the multigram synthesis of Disarib (Scheme 2) was developed.

2.2. *The process improved scalable synthesis of Disarib Ls through Scheme 2*

The new strategic approach used for the multigram synthesis was

discussed in Scheme 2. During the scale-up synthesis, we used $POCl_3$ as a reagent for cyclization in step 1 instead of sulfuric acid to improve the yield. As a result, yield improved from 55 % to 96.2 %. 5-(4-chlorobenzyl)-1,3,4-thiadiazol-2-amine **(3)** was synthesized from commercially available 2-(4-chlorophenyl)acetic acid (1 kg, 5.86 mol) **(1)** and thiosemicarbazide (0.587 kg, 6.44 mol) **(2),** which was thoroughly mixed, and charged portion-wise into phosphorous oxychloride ($POCl_3$) (5 L) at ambient temperature. After the addition, the reaction mixture was heated to 75–80 °C for 3 h. The reaction mass was gradually cooled to 25–30 °C and stirred for 2 h. The progress of the reaction was monitored by HPLC [IPC Limit: 4-chlorophenylacetic acid should not be more than 5 %, and thiosemicarbazide should not be more than 10 %]. After the completion of the reaction, the reaction mass was quenched on ice (60 kg) and stirred the mixture for 30 min at 5–10 °C. The pH of the reaction mass was then adjusted to 8–9 using 50 % aq. sodium hydroxide solution (22 L) and then stirred for 30 min. The off-white product formed was filtered and washed with water until the pH of the last MLR became neutral. The solid was unloaded and dried under a hot air oven at 50–55 °C for 5 h (1.27 kg). The structure of the intermediate **(3)** was confirmed through ^{1}H NMR (Fig. S1A), ^{13}C NMR (Fig. S1B), LCMS (Fig. S1D) and HRMS (Fig. S1E) analysis. The product was obtained as an off-white solid with a purity of 98 % (HPLC analysis, area%) (Fig. S1C) and a yield of 96.2 %.

The next stage was the key step of the synthesis because the condensation and formylation reactions were carried out in a single step via the "Domino reaction" [48]. When 5-(4-chlorobenzyl)-1,3,4-thiadiazol-2-amine (1 kg, 4.43 mol) **(3)** was dissolved in DMF (10 L) and treated with 4-bromophenacyl bromide (1.232 kg, 4.43 mol) **(4)**, it undergoes condensation reaction at 115–120 °C which leads to the *in situ* generation of intermediate 5. The reaction was monitored by HPLC [IPC limit: compound (3) should not be more than 0.5 %]. Immediately after the complete consumption of compound **3**, a formylation reaction was carried out *in situ* without isolating intermediate **5** by using phosphorous oxychloride ($POCl_3$) (3.75 L), which was added to the reaction mass while maintaining the temperature below 5 °C. After the completion of the addition of $POCl_3$, the reaction mass was further stirred at 5–10 °C for 30 min and then heated to 60–65 °C for 1 h. The progress of the reaction was monitored by HPLC [IPC limit: intermediate (5) should not be more than 0.5 %]. After the completion of the reaction, the reaction mixture was gradually cooled to 25–30 °C and then quenched in DM water (50 L), and the obtained solid was stirred for 30 min and then filtered. Later, the solid with DM water (10 L) was subjected to basification with 1 % sodium carbonate solution (10 L), and washed with DM water (10 L) until the pH of the last MLR became neutral. Then, the obtained solid was dried in a hot air oven at 50–55 °C. The crude product **(6)** was purified using ethanol (12 L). The crude product was suspended in ethanol (12 L) and heated to 60–65 °C for 30 min, and the reaction mixture was gradually cooled to 35–40 °C and filtered. Washed the solid with ethanol (3 L) and dried it in a hot air oven at 50–55 °C for 6 h. The structure of the intermediate **(6)** was confirmed through ^{1}H NMR (Fig. S2A), ^{13}C NMR (Fig. S2B), LCMS (Fig. S2D) and HRMS (Fig. S2E) analysis. The product (1.46 kg) obtained was 99.5 % pure, as determined based on HPLC (Fig. S2C), at a yield of 76 %.

In the final step (condensation), 6-(4-bromophenyl)-2-(4-chlorobenzyl)imidazo[2,1-b] [1,3,4]thiadiazole-5-carbaldehyde (0.6 kg 1.38 mol) **(6)** and oxindole (0.203 kg, 1.52 mol) **(7)** was dissolved in ethanol (12 L) and piperidine (0.141 kg, 1.66 mol) was added dropwise at 25–30 °C. The reaction mixture was then heated over an oil bath under stirring with an overhead stirrer to 70–75 °C and maintained for 3–5 h. Using HPLC analysis the progress of the reaction was monitored until the compound **(6)** was not more than 1 %. After the completion of the reaction, the reaction mass was gradually cooled to 40–45 °C and filtered the yellowish-colored solid. The obtained solid was washed with ethanol (3 L) and suck-dried, followed by a slurry washed with DM water (12 L), and then suck-dried under reduced pressure for 1 h, followed by drying in a hot air oven at 50–55 °C till constant weight to give yellowish colored solid (0.660 kg). The structure of the product Disarib **(8)** was confirmed through ^{1}H NMR (Fig. 2A), ^{13}C NMR (Fig. 2B), LCMS (Fig. 2D) and HRMS (Fig. 2E) analysis. The product was obtained with a purity of 98.8 % (HPLC analysis) (Fig. 2C) with a yield of 86.8 %.

Thus, the developed scalable synthetic pathway (Scheme 2) of Disarib resulted in a yield of 86.8 % with 98.8 % HPLC purity. Using $POCl_3$ as a reagent for cyclization in step 1 instead of H_2SO_4 and using DMF as a solvent instead of ethanol in step 2 resulted in the process optimization followed by higher yields. The improved purity of the product was analyzed using HPLC. Combining the condensation and formylation reactions (step 2 and step 3) from Scheme 1 into the single flux domino reaction contributed to reducing the overall higher cycle time of the Disarib synthesis process. The 85 % yield of Disarib synthesized through Scheme 1 improved to 86.8 % through Scheme 2, and the purity analysis by HPLC for Disarib (Scheme 2) showed an improved purity of 98.8 % in comparison with the 91.6 % purity obtained for Disarib (Scheme 1). Thus, Scheme 2 provided a practical, cost-effective, and scalable synthetic method for Disarib.

2.3. *Biophysical characterization of Disarib Ss synthesized using ^{1}H NMR spectroscopy and HPLC analysis*

Proton NMR spectroscopy and HPLC are used for the analytical characterization of various biochemical molecules [17,54]. NMR spectroscopy is used for structural determination and HPLC analysis involves the detection, quantification and purity of chemicals of interest. Here, we have analyzed Disarib synthesized through Scheme 1 using ^{1}H NMR spectrum and the HPLC analysis. The ^{1}H NMR spectrum of Disarib Ss confirmed the structure of the synthesized product, and it was identical to the previously reported NMR spectrum of Disarib [15]. The peaks obtained for the ^{1}H NMR (400 MHz, DMSO-d_6- *solvent*) of Disarib (Scheme 1) are: δ 10.65 (s, 1H); 7.62 (m, J = 8 Hz, 4H); 7.53 (s, 1H); 7.37

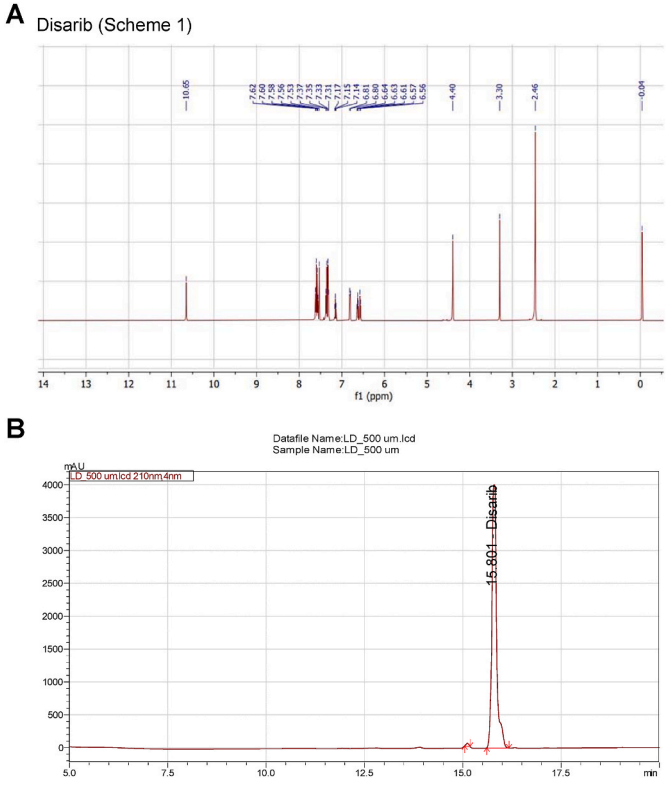

Fig. 1. Biophysical characterization of Disarib Ss. A. The 1H NMR Spectrum of Disarib Ss (in-house) was used to elucidate the chemical structure. B. HPLC analysis of Disarib, synthesized through Scheme 1, was used to detect and test the purity of Disarib.

(m, $J = 8$, 4H); 7.17 (t, $J = 8.0$ Hz, 1H); 7.14 (d, $J = 8.0$ Hz, 1H); 6.80 (t, $J = 8$ Hz, 1H); 6.57 (d, $J = 8$ Hz 1H); 4.40 (s,1H) (Fig. 1A). The detection and quantification of Disarib Ss using HPLC analysis unveiled a peak of Disarib around a retention time (RT) of 15.801 min (Fig. 1B). The HPLC purity of the obtained Disarib was determined to be 91.6 % (Fig. 1B).

2.4. Biophysical characterization of Disarib Ls using ^{1}H NMR, ^{13}C NMR, HPLC analysis, LCMS, HRMS, FT-IR, and UV–Vis spectroscopy

The characterization of the final product, Disarib, obtained through Scheme 2 was done using ^{1}H NMR spectroscopy, ^{13}C NMR spectroscopy, HPLC analysis, LCMS analysis, HRMS analysis, FT-IR spectroscopy, and UV–Vis spectroscopy. The ^{1}H NMR spectrum of Disarib Ls was comparable with the ^{1}H NMR spectrum obtained for Disarib Ss (Fig. 2A). The peaks obtained for the ^{1}H NMR (400 MHz, DMSO-d_6- *solvent*) of Disarib (Scheme 2) are: δ 10.67 (s, 1H); 7.66 (m, $J = 8.8$ Hz, 4H); 7.57 (s, 1H); 7.41 (m, $J = 8.8$,4H); 7.19 (t, $J = 8.0$ Hz, 1H); 6.86 (d, $J = 8.0$ Hz, 1H); 6.67 (t, $J = 7.2$ Hz, 1H); 6.61 (d, $J = 7.6$ Hz 1H); 4.43 (s,1H). Thus, the structure of Disarib synthesized through both Schemes was confirmed (Figs. 1A and 2A). The structure of Disarib Ls was further confirmed using ^{13}C NMR spectroscopy (Fig. 2B). The peaks obtained for the ^{13}C NMR (100 MH_Z, DMSO-d_6-solvent) of Disarib (Scheme 2) are: δ 168.341, 164.950, 147.567, 144.502, 142.810, 134.843, 132.977, 132.165, 131.687, 130.829, 130.040, 128.705, 124.706, 121.398, 120.935, 120.670, 118.765, 117.559, 109.630, 36.078. The HPLC analysis of Disarib (Scheme 2) revealed a peak of Disarib around retention time (RT) of 13.289 min (Fig. 2C). The HPLC purity of the obtained Disarib was determined to be 98.8 % (Fig. 2C). Increase in the HPLC purity was observed for Disarib Ls in comparison to Disarib Ss (Fig. 1B; 2C). A marginal difference in the RT was observed between both batches of Disarib. Mass spectrometry analysis (LCMS) of Disarib provided further confirmation on Disarib structure as MS (ESI): $m/z = 548.8$ [M+1], (Fig. 2D).

HRMS analysis has been done for the compound identification and structure elucidation; HRMS (ESI) m/z: $[M + H]^{+}$calcd for $C_{26}H_{16}BrClN_4OS$: 548.8550; found: 549.0025 (Fig. 2E). The FT-IR spectroscopy analysis of Disarib Ls revealed, (υ_{max}, cm^{-1}): 3172, (N–H stretching), 3089 (Aromatic CH), 1705 (C═O stretching) peaks (Fig. 2F). Disarib was evaluated using a UV–visible spectrophotometer to obtain chemical properties and electronic structure of the compound. The maximum absorption for Disarib was observed at 380 nm (Fig. 2G), indicating the presence of a conjugated pi-electron system of the aromatic ring structure.

2.5. Disarib synthesized through Scheme 2 showed comparable cytotoxic effects in BCL2-high cancer cell lines

The Disarib synthesized through large-scale synthetic pathway (Scheme 2) was analyzed for its cytotoxic effect in three leukemic cell lines expressing higher levels of BCL2 (MOLT4, CEM, NALM6). The results showed that the cell viability was significantly reduced when treated with increasing concentration of Disarib Ls (48 h), comparable with the effect shown by Disarib synthesized using Scheme 1 (Fig. 3A and B). A significant reduction in the % of cell viability was observed between 1 and 5 μM concentrations of Disarib Ls and Disarib Ss in the MOLT4 cell line. Comparable results were obtained for the CEM cell line, where both batches of Disarib showed similar cytotoxic effects and showed a significant reduction in cell viability between 1 and 5 μM. A concentration-dependent decrease in the cell viability was observed in the NALM6 cell line with a remarkable reduction in cell viability between concentrations 1 and 5 μM. Thus, both batches of Disarib have shown comparable cytotoxic effects in BCL2 high cancer cell lines, which is in line with our previous studies on BCL2-dependent cytotoxic effect shown by Disarib in various cancer cell lines [15,49].

2.6. Disarib Ls induced cell death without inducing cell cycle arrest

Previously, we have shown that Disarib does not induce cell cycle arrest in cancer cell lines [49]. Based on that, we were interested in testing the effect of Disarib Ls on the cell cycle progression. To investigate this, MOLT4 cells were treated with increasing concentrations of Disarib Ls (0, 1, 2, and 5 μM for 48 h) synthesized through Scheme 2, and the effect was compared with Disarib Ss following staining with Propidium Iodide and FACS analysis (Fig. 4). The results showed a significant increase in the cells in the sub-G1 phase of the cell cycle when increasing concentration of Disarib was treated, indicating cell death in the case of Disarib Ls. However, we could not observe any cell cycle phase-specific arrest at any concentration (Fig. 4), which was consistent with our previous results. Thus, our results revealed that Disarib Ls and Disarib Ss showed similar effects on the cell cycle progression.

2.7. Disarib Ls and Disarib Ss showed comparable effects on tumor regression in EAC mouse models

Previous studies have shown that Disarib induces a significant tumor reduction in various tumor models with minimal side effects in treated animals [30,40,41,49]. Besides, we compared the oral and intraperitoneal (IP) routes of Disarib administration in the EAC tumor model, which showed that tumor regression efficacy of Disarib administered intraperitoneally was comparable with that of oral administration of Disarib when 50 mg/kg b.wt. of Disarib was administered [40].

Syngeneic mouse models, Ehrlich ascites breast carcinoma (EAC) showed sensitivity to Disarib when a maximal dose of 50 mg/kg was administered orally [40]. Therefore, we were interested in comparing the tumor regression efficacy of Disarib Ls, in the EAC mouse model when administered orally and intraperitoneally. The solid tumors were generated by injecting EAC cells in the thigh region of 6 to 8-week-old Swiss albino mice. Disarib was administered through both oral and intraperitoneal routes (Fig. 5A). Based on previous results, an intraperitoneal dose of Disarib Ls (10 mg/kg b. wt.) was given for a total of 6 days (every alternate day), the oral dosing was given for continuously for 14 days (50 mg/kg b. wt.) [15,40,49]. Once a visible tumor was seen in mice, the tumor growth was recorded for a period of 24 days. The results showed a significant decrease in tumor growth following treatment with Disarib Ls in the EAC mouse model (Fig. 5B and C). Importantly, both Disarib Ls and Ss showed comparable efficacy in tumor regression by both the route of administration (intraperitoneal or oral) performed (Fig. 5B and C). This suggests that the Disarib synthesized through both routes possesses comparable efficacy in inhibiting tumor growth.

2.8. Effect of Disarib synthesized through Scheme 2 on the histopathology of tissues derived from EAC mouse models

Disarib Ls has shown remarkable tumor regression efficacy when administered orally and intraperitoneally in both tumor models [40,49]. Further, we were interested in conducting histopathological studies using tumor tissues from the animals treated with Disarib Ls. EAC-injected Swiss albino mice were treated with Disarib in oral (50 mg/kg b. wt, 14-day continuous dose) and IP (10 mg/kg b. wt, 6 doses, alternate days) routes. After 24 days, we collected the tumor samples from control and Disarib-treated mice and kidney and liver tissues since these organs are involved in the direct absorption and excretion of drugs [49]. The HE staining of tumor tissues derived from Disarib-treated animals showed fewer infiltrated cells than the control tumor tissue. Also, the HE staining of liver and kidney sections of treated animals showed no irregularity, which indicates an absence of side effects upon Disarib administration. It was also found that both oral and IP ways of Disarib administration did not differ in the histopathology of derived tissue sections (Fig. 6A and B). Thus, histopathological analysis of multiple organs revealed that treatment with Disarib synthesized

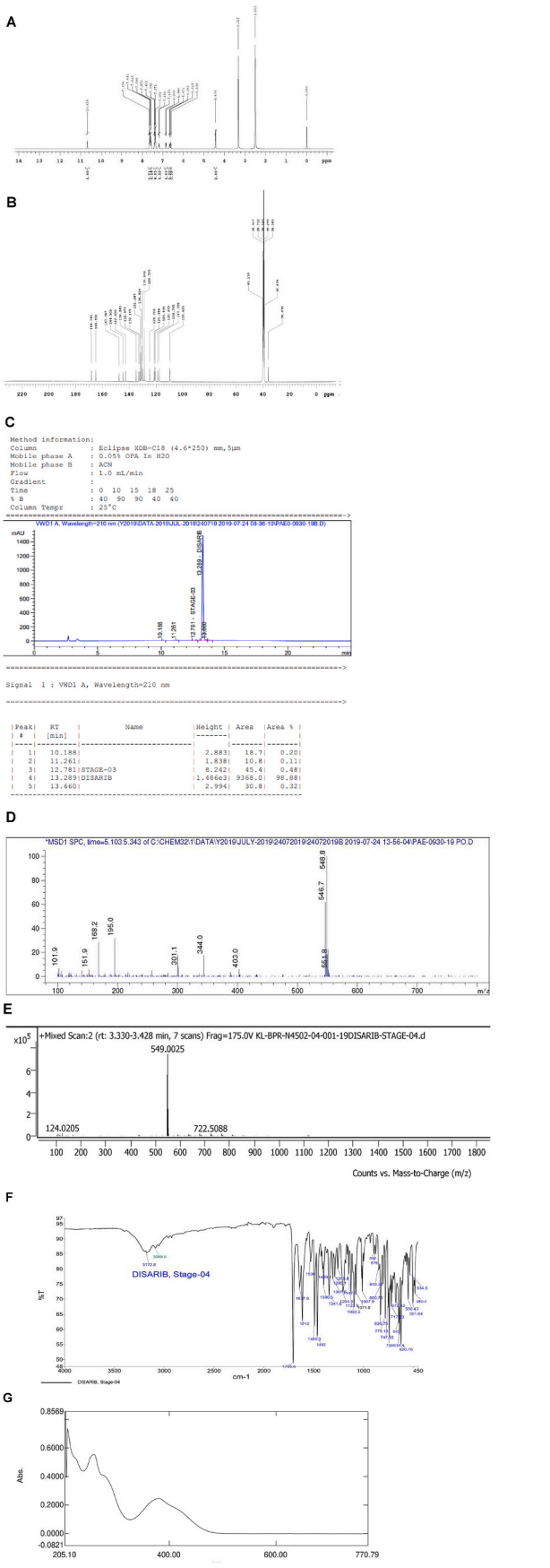

(caption on next column)

Fig. 2. Biophysical characterization of Disarib Ls. A. ^{1}H NMR Spectrum of Disarib Ls (large-scale synthesis in GLP-certified laboratory) used for the structure elucidation of the compound. B.^{13}C NMR Spectrum of Disarib Ls. C. HPLC analysis of Disarib synthesized through Scheme 2. D. LCMS Spectrum of Disarib Ls. E. HRMS Spectrum of Disarib Ls was used for the compound identification and structural elucidation. F. FT-IR Spectrum of Disarib Ls. G. UV–Vis spectrum of Disarib was used for the compound identification and characterization.

through Scheme 2 did not affect the normal architecture of the liver and kidney. These results were comparable with the previous observations that we obtained for the histopathological studies using Disarib Ss (Scheme 1) [49]. Thus, results showed that Disarib administration leaves no anomaly in the histopathology of various organs indicating no side effects.

2.9. The pharmacokinetic analysis of Disarib indicated its highest bioavailability after 4 h of administration in mice

Understanding the pharmacokinetic profile of a compound plays a pivotal role in the drug development process [2] as it can shorten the overall timeline during the early clinical trial initiation. In our preceding work, we investigated the pharmacokinetic profile of Disarib Ls in the serum of Swiss albino mice after Disarib administration. Disarib Ls, when administered intraperitoneally (10 mg/kg b. wt.) in Swiss albino mice, prompted a rapid attainment of peak serum concentration, Cmax of 26.3 µg/ml within 30 min, indicating the swift *in vivo* absorption kinetics of Disarib along with a brief half-life of 2.3 h [49]. These results were comparable with that of Disarb Ss.

To understand the pharmacokinetic characteristics of Disarib Ls, we conducted the present study in Swiss albino mice, administering it orally at a dose 50 mg/kg body weight (Fig. 7A). We compared the pharmacokinetics of Disarib Ls with Disarib Ss (Fig. 7). Serial serum samples were collected from the mice at intervals ranging from 15 min to 72 h after oral administration of Disarib Ls and Disarib Ss. The concentrations of Disarib in the serum were quantified using HPLC LabSolutions software. Calculating the area under the concentration-time curve (AUC) provided insights into the compound's pharmacokinetic profile. HPLC analysis of Disarib Ls revealed a peak serum concentration (Cmax) of approximately 4–5 µg/ml, occurring at 4–6 h (Tmax) after oral administration. This pharmacokinetic profile was comparable to that of Disarib Ss (Fig. 7B and C). Importantly, Disarib exhibited an extended half-life (t1/2) of 12 h in the serum of Swiss albino mice. These parameters offer significant insights into the Disarib's distribution within the body, its rate of elimination driven by equilibrium, and provide a foundational basis for the requirements of forthcoming clinical trials.

3. Materials and methods

3.1. Chemicals and reagents

Chemical reagents used in this study were obtained from Sigma Chemical Co. (St. Louis, MO, USA) and SRL (Andheri (E), Mumbai, India). Culture media were from Sera Laboratory International Limited (West Sus-sex, UK), and FBS and PenStrep were from Gibco BRL (Gaithersburg, MD, USA).

3.2. NMR spectroscopy

^{1}H NMR spectra were recorded on a 400 MHz NMR spectrometer. Chemical shifts are reported in ppm relative to tetramethylsilane; coupling constants (J) are reported in hertz, referred to as apparent peak multiplicities. ^{13}C NMR spectroscopy analyses were recorded on a 100 MHz spectrometer. DMSO-d_6 was used as a solvent for dissolving the samples. The obtained ^{1}H and ^{13}C NMR spectra of the compounds were analyzed using MestreNova x 64 (Mnova) software.

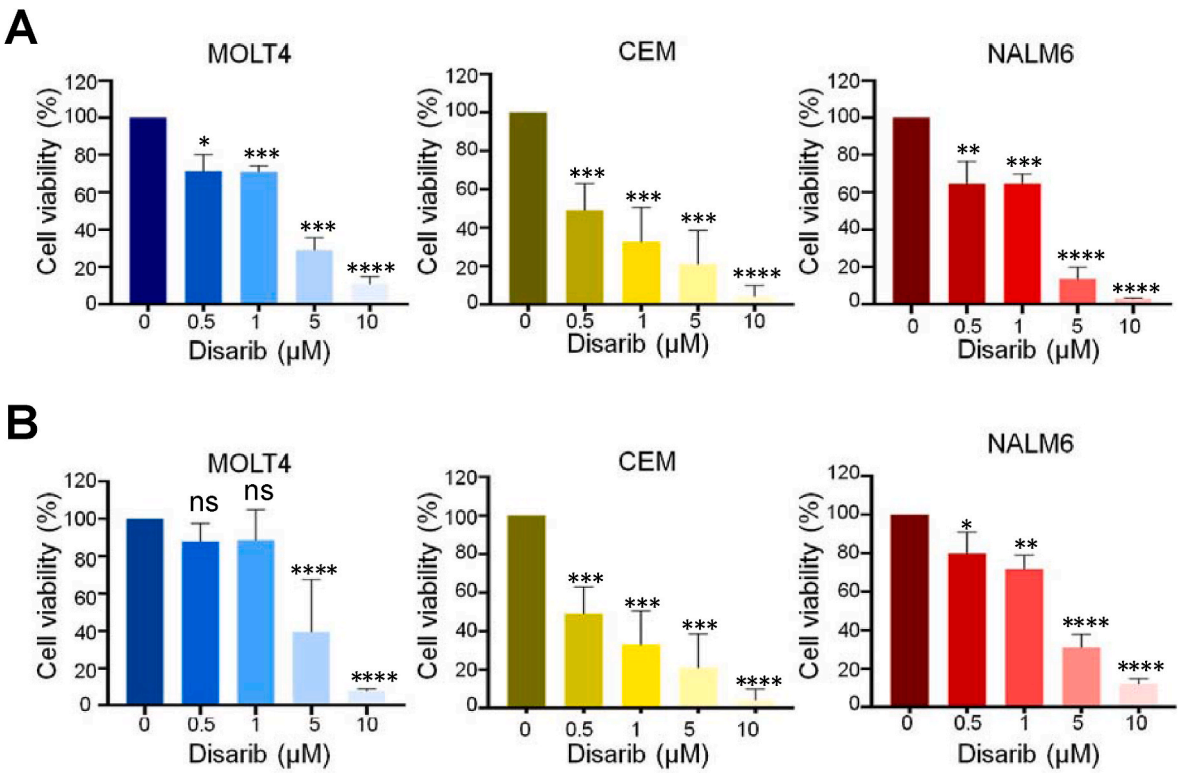

C

Cell lines	Scheme 1 IC_{50} (μM)	Scheme 2 IC_{50} (μM)
MOLT4	2.7	3.2
CEM	1.26	1.26
NALM6	1.95	2.9

Fig. 3. Evaluation of comparison of the cytotoxicity in various BCL2 high cancer cell lines induced by Disarib, synthesized through Schemes 1 and 2. A. Evaluation of cytotoxicity following 48 h of treatment with Disarib Ss in MOLT4, CEM, and NALM6 cells (0.5, 1, 5, and 10 μM). Cell death was assayed by trypan blue dye exclusion assay. Experiments were performed at least three times, and the graph shown represents mean ± SEM. B. Evaluation of cytotoxicity following treatment with Disarib Ls in MOLT4, CEM, and NALM6 cells (0.5, 1, 5, and 10 μM for 48 h). Experiments were performed a minimum of three times, and the graph shows mean ± SEM. C. Table showing the comparison of IC_{50} values of Disarib synthesized through Scheme 1 and Scheme 2 based on their cytotoxicity in MOLT4, CEM, and NALM6. IC_{50} values were based on the results presented in panels A and B. The experiments were performed at least three times; data are presented in mean ± SEM. (For interpretation of the references to color in this figure legend, the reader is referred to the Web version of this article.)

3.3. Chemical synthesis

All reactions were carried out in oven-dried glassware under an atmosphere of nitrogen. The commercially available starting materials were used as received without further purification, and all solvents were dried by standard methods prior to use.

3.3.1. 5-(4-chlorobenzyl)-1,3,4-thiadiazol-2-amine (3)

2-(4-chlorophenyl)acetic acid (1 kg, 5.86 mol) and thiosemicarbazide (0.587 kg, 6.44 mol) were thoroughly mixed and charged portion-wise into phosphorous oxychloride ($POCl_3$) (5 L) in a RBF under efficient stirring at ambient temperature. Heated the reaction mixture to 75–80 °C for 3 h. Cooled the reaction mass gradually to 25–30 °C and stirred for 2 h. The reaction was monitored by HPLC [4-chlorophenylacetic acid should not be more than 5 % and thiosemicarbazide should not be more than 10 %]. Quenched the reaction mass into ice (60 kg) and stirred the mixture for 30 min at 5–10 °C. The pH of the reaction mass was then adjusted to 8–9 using 50 % aq. sodium hydroxide solution (22 L) and then stirred for 30 min. The off-white product formed was filtered and washed with water until the pH of the last MLR became neutral. The solid was unloaded and dried under a hot air oven at 50–55 °C for 5 h to give 1.27 kg; Yield: 96.2 %. The product was obtained with a purity of 98 % (HPLC analysis). ^{1}H NMR (400 MHz, DMSO-d_6): δ 7.39 (d, J = 7.2Hz, 2H); 7.31 (d, J = 7.6 Hz, 2H); 7.05 (s, 2H); 4.15 (s, 2H); MS (ESI): m/z = 225.8 [M]. ^{13}C NMR (100 MHz, DMSO-d_6): δ 168.933, 156.945, 137.013, 131.535, 130.518, 128.561, 34.674 (Fig. S1B). HRMS (ESI) m/z: [M +H]$^+$calcd for $C_9H_8ClN_3S$; 226.6940; found: 226.0134 (Fig. S1E).

3.3.2. 6-(4-bromophenyl)-2-(4-chlorobenzyl)imidazo[2,1-b] [1,3,4] thiadiazole-5-carbaldehyde(6)

5-(4-chlorobenzyl)-1,3,4-thiadiazol-2-amine (1 kg, 4.43 mol) (3) was

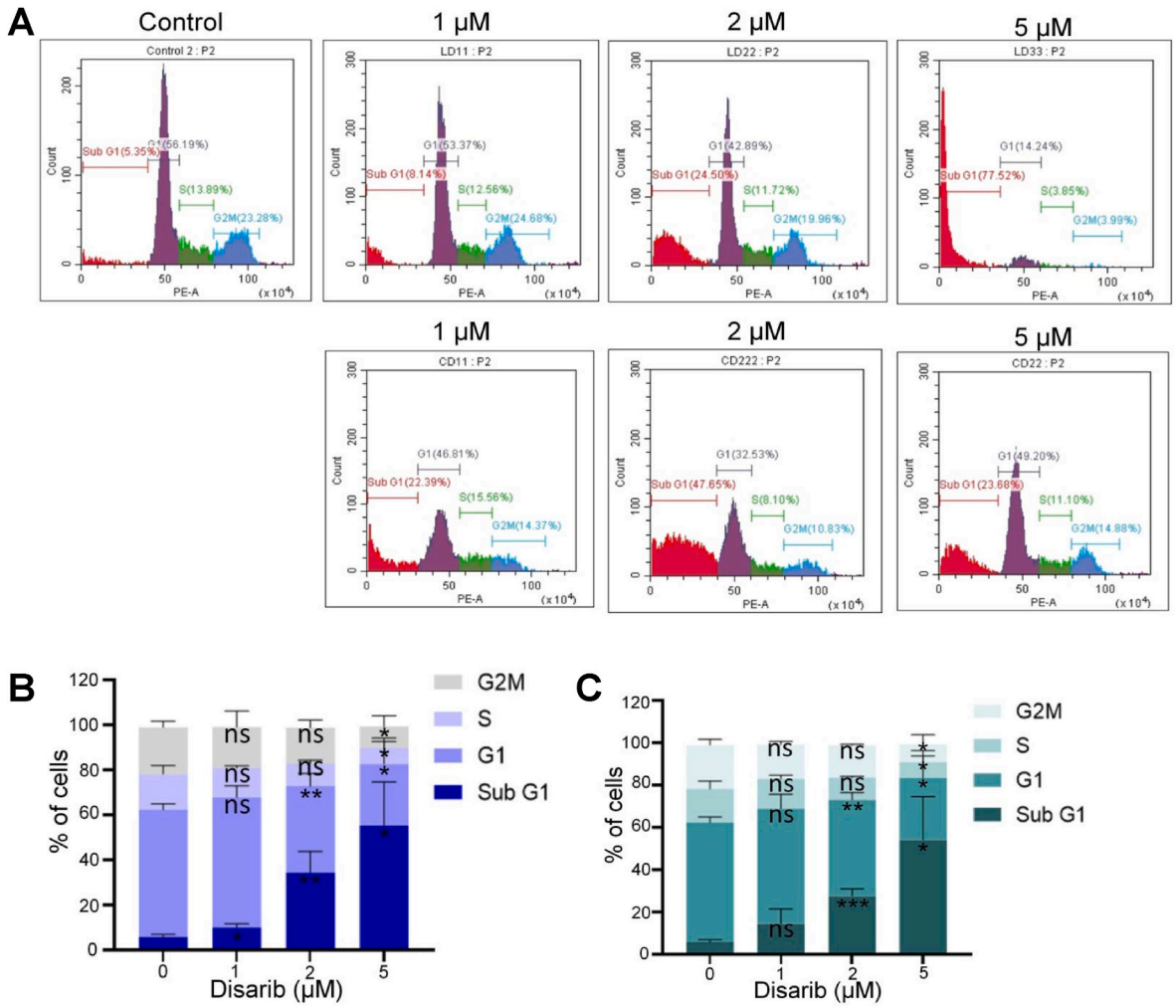

Fig. 4. Evaluation of the effect of Disarib, synthesized through Scheme 1 and Scheme 2, on cell cycle progression. A. Cell cycle analysis following treatment with Disarib Ss (upper panel) and Disarib Ls (lower panel) in MOLT4 cells (1, 2, and 5 μM for 48 h). B, C. The bar graph represents the relative quantification of the percentage of cells in each phase of the cell cycle after treatment with Disarib from Scheme 1 (B) and Scheme 2 (C). Each experiment was independently repeated a minimum of three times, and error bars indicate the mean ± SEM. (ns: not significant, *p < 0.05, **p < 0.005, ***p < 0.0001).

dissolved in DMF (10 L) and treated with 4-bromophenacyl bromide (1.232 kg, 4.43 mol) under efficient stirring. The reaction mass was heated to 115–120 °C for 3 h. The reaction was monitored by HPLC [compound (5) should not be more than 0.5 %]. Cooled the reaction mixture gradually to 5–10 °C and stirred for 10–15 min. Phosphorous Oxychloride ($POCl_3$) (3.75 L) was charged drop-wise into the reaction mass while maintaining the temperature below 10 °C. After completion of addition the reaction mass was further stirred at 5–10 °C for 30 min and then heated to 60–65 °C for 1 h. The reaction was monitored by HPLC [intermediate (5) should not be more than 0.5 %]. The reaction mixture was then gradually cooled to 25–30 °C and then quenched in DM water (50 L). Stirred the solid for 30 min and then filtered. Washed the solid with DM water (10 L), basified with 1 % sodium carbonate solution (10 L), and then washed with water (10 L) until the pH becomes neutral. The solid was then dried in a hot air oven at 50–55 °C. The crude product was then treated with ethanol (12 L) at 60–65 °C for 30 min. Cooled the reaction mixture gradually to 35–40 °C and then filtered. Washed the solid with ethanol (3 L) and dried in hot air oven at 50–55 °C for 6 h to give 1.46 kg; Yield: 76.04 %. The product was obtained with a purity of 99.5 % (HPLC analysis). ^{1}H NMR (400 MHz, DMSO-*d6*): δ 9.99 (s, 1H); 7.93 (d, J = 8.4 Hz, 2H); 7.73 (d, J = 8.0 Hz, 2H); 7.46 (s, 4H); 4.57 (s, 2H); MS(ESI): m/z = 433.8 [M+1]. ^{13}C NMR (100 MHz, DMSO-d_6): δ 177.037, 166.885, 152.074, 150.496, 134.775, 132.332, 131.573, 131.330, 130.981, 130.587, 128.819, 123.363, 123.113, 35.972 (Fig. S2B). HRMS (ESI) m/z: [M +H]$^+$calcd for $C_{18}H_{11}BrClN_3OS$; 433.7200; found: 433.9629 (Fig. S2E).

3.3.3. 3-((6-(4-bromophenyl)-2-(4-chlorobenzyl)imidazo[2,1-b] [1,3,4] thiadiazol-5-yl)methylene)indolin-2-one (8) (Disarib)

6-(4-bromophenyl)-2-(4-chlorobenzyl)imidazo[2,1-b] [1,3,4] thiadiazole-5-carbaldehyde (0.6 kg 1.38 mol) and oxindole (0.203 kg, 1.52 mol) was taken in ethanol (12 L) at 25–30 °C and added dropwise piperidine (0.141 kg, 1.66 mol) over 20 min. The reaction mixture was then heated over an oil bath under stirring with an overhead stirrer to 70–75 °C and maintained for 3–5 h. The reaction mixture monitored through HPLC till compound (6) was not more than 1 %. The reaction mass was then gradually cooled to 40–45 °C and filtered the yellowish colored solid through cloth; washed with ethanol (3 L); suck dried followed by made slurry wash with DM water (12 L); suck dried under reduced pressure for 1 h followed by dried in hot air oven at 50–55 °C till constant weight to give yellowish colored solid with weight 0.660 kg; Yield: 86.88 %. The product was obtained with a purity of 98.8 % (HPLC analysis). ^{1}H NMR (400 MHz, DMSO-d_6): δ 10.67 (s, 1H); 7.66 (m, J = 8.8 Hz, 4H); 7.57 (s, 1H); 7.41 (m, J = 8.8,4H); 7.19 (t, J = 8.0 Hz, 1H); 6.86 (d, J = 8.0 Hz, 1H); 6.67 (t, J = 7.2 Hz, 1H); 6.61 (d, J = 7.6 Hz 1H); 4.43 (s,1H). MS (ESI): m/z = 548.8 [M+1]. 13C NMR (100 MHZ, DMSO-d_6-solvent) of Disarib (Scheme 2) are: δ 168.341, 164.950, 147.567, 144.502, 142.810, 134.843, 132.977, 132.165, 131.687, 130.829,

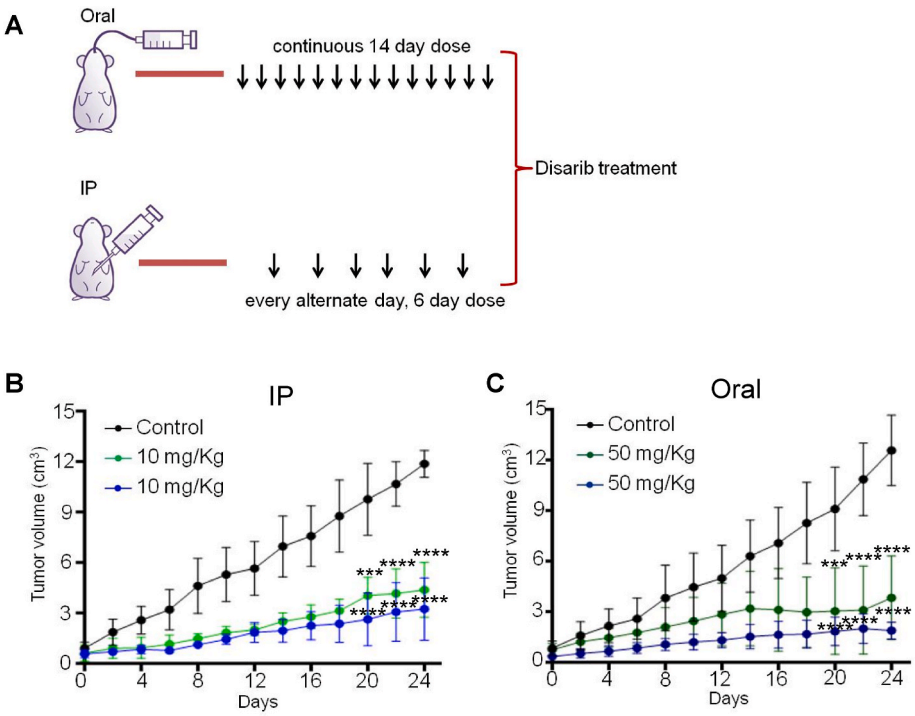

Fig. 5. Comparison of efficacy of Disarib Ls with Disarib Ss on tumor regression in different tumor models. A. Schematic representation of the two distinct routes used for administering Disarib. In one approach, Disarib was administered orally for 14 consecutive days. Alternatively, Disarib was administered intraperitoneally, with intervals of every alternate day for 6 days. B. Graph depicting the *in vivo* progression of breast adenocarcinoma upon intraperitoneal administration of Disarib. The solid tumors were generated by injecting EAC cells in the thigh region of Swiss albino mice (6–8 weeks old), which were then intraperitoneally treated with Disarib (10 mg/kg, 6 doses, alternate days). Tumor volume was plotted against a period of 24 days. The green line represents the effect of Disarib synthesized through Scheme 1 on EAC tumor progression. The blue line represents the effect of Disarib synthesized through Scheme 2 on EAC tumor progression. C. Graph depicting the *in vivo* progression of breast adenocarcinoma upon oral administration of Disarib. The solid tumors were generated by injecting EAC cells in the thigh region of 6 to 8-week-old Swiss albino mice, which were then orally treated with Disarib (50 mg/kg, continuous 14 days of dosing). Tumor volume was plotted against a period of 24 days. The green line represents the effect of Disarib synthesized through Scheme 1 on EAC tumor progression. The blue line represents the effect of Disarib synthesized through Scheme 2 on EAC tumor progression. (For interpretation of the references to color in this figure legend, the reader is referred to the Web version of this article.)

130.040, 128.705, 124.706, 121.398, 120.935, 120.670, 118.765, 117.559, 109.630, 36.078 (Fig. 2B). HRMS (ESI) *m/z*: $[M+H]^+$calcd for $C_{26}H_{16}BrClN_4OS$; 548.8550; found: 549.0025 (Fig. 2E).

3.4. Liquid Chromatography-Mass Spectrometry (LCMS)

For LCMS analysis, the samples were analyzed using a LC/MSD TOF (time-of-flight) mass spectrometer in an electrospray positive ionization mode via flow injection. The column used was Zorbax SB C8 (75mmX4.6 mm) 3.5 µ. The mobile phase A consisted of 0.1 % Formic acid in water, and the mobile phase B used was Acetonitrile. The injection volume used was 5.00 µl, and the flow rate was 1.0 ml/min.

3.5. High-Resolution Mass Spectrometry (HRMS)

The samples were analyzed using the MS-type TOF (time-of-flight). The column used was Poroshell 120 EC-C18 (50*3.0) mm, 2.7 µm. The mobile phase A consisted of 0.1 % Formic acid in water, and mobile phase B was 0.1 % Formic acid in Acetonitrile. The injection volume was 0.2 µl, and the flow rate was 0.8 ml/min. The obtained results were analyzed using the mass spec screening software MassHunter Qualitative Analysis.

3.6. Fourier-Transform Infrared Spectroscopy (FT-IR)

The FT-IR analysis of the sample was measured using a PerkinElmer Spectrum FTIR spectrometer. The spectra analysis of the samples was done using PerkinElmer Spectrum IR ES Version 10.6.2.

3.7. Ultraviolet–visible spectroscopy (UV–Vis)

For the UV–Vis spectroscopy analysis, the samples were analyzed in UV-1800, Shimadzu spectrophotometer, at the wavelength range of 200 nm–800 nm. The obtained results were analyzed using LabSolutions UV–Vis, an analytical data system.

3.8. Cell lines and culture

MOLT4 (T-cell leukemia) was purchased from the National Centre for Cell Science, Pune, India. CEM (T-cell leukemia) and NALM6 (B-cell leukemia) were kind gifts from Dr. M.R. Leiber, USA. Cells were cultured in RPMI 1640 medium supplemented with 10 % FBS, 100 µg ml^{-1} Penicillin, and 100 µg streptomycin.ml^{-1} and incubated at 37 °C in a humidified atmosphere containing 5 % CO_2.

3.9. Trypan blue exclusion assay

Cell viability after treatment with Disarib was assayed using trypan blue exclusion assay [15,31,51]. Briefly, the two different batches of Disarib (0.5, 1, 5, 10 µM) were added to the cells (MOLT4, CEM, NALM6) and were harvested at 48 h post-treatment. A number of viable cells were ascertained by mixing cells with an equal volume of 0.4 % trypan blue stain (Sigma Chemical Co.). The cells were then counted using a hemocytometer, and the cell number was plotted against the time period of cell growth. Data from the 48 h time point was used to calculate the IC_{50} value of two compound batches from selected cell lines. DMSO-treated cells served as the vehicle control. The results

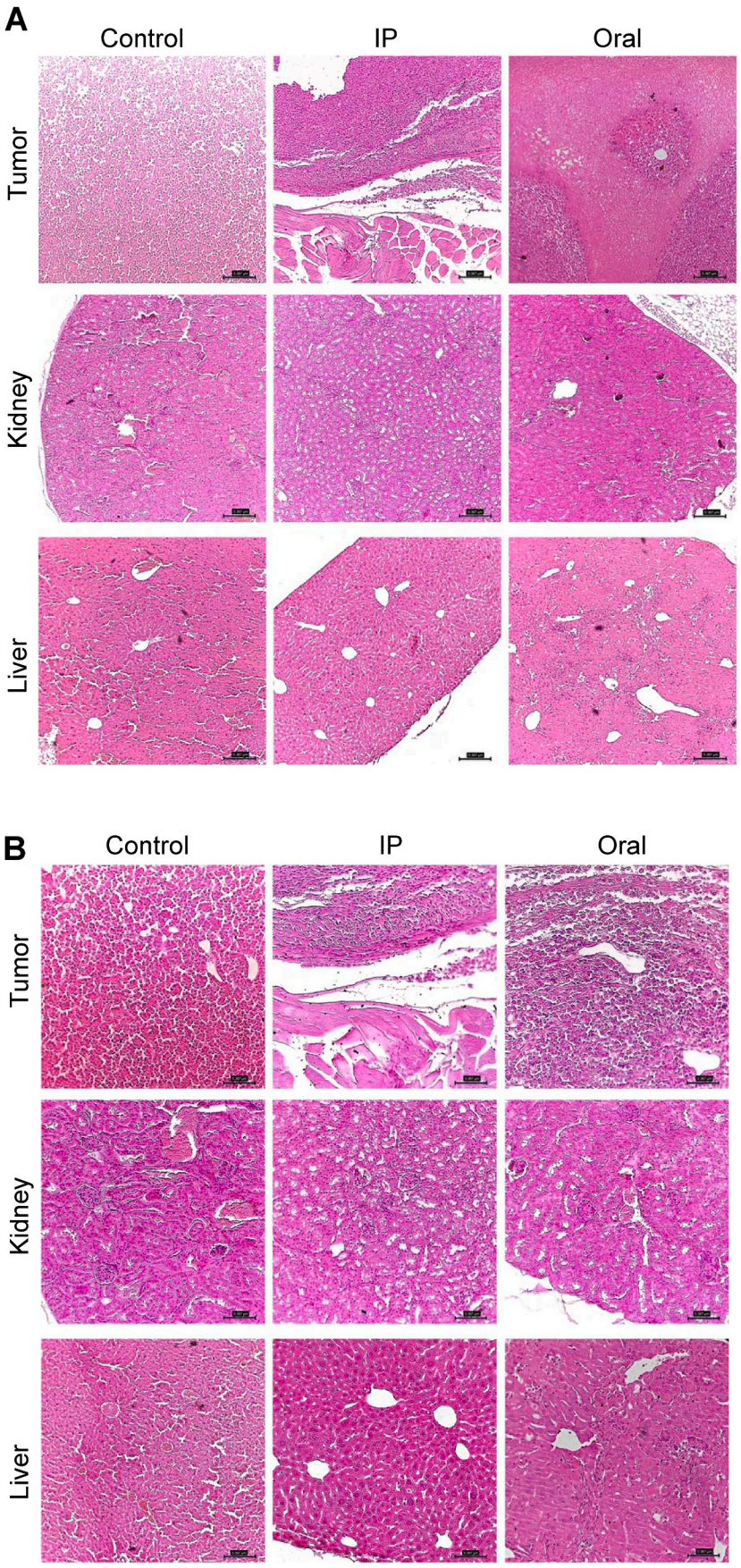

(caption on next page)

Fig. 6. Histopathological analysis of different tissues of mice following oral and intraperitoneal administration of Disarib Ls. A, B. HE staining of tumor, kidney, and liver tissues from control and Disarib administered mice (IP, 10 mg/kg b. wt. and oral, 50 mg/kg b. wt.). Images are shown with 10X (A) and 20× (B) magnifications. In all panels, "control' indicates tissues derived from mice with tumors, and "IP and Oral" indicates mice with tumors after treatment with Disarib Ls and administered through two different routes.

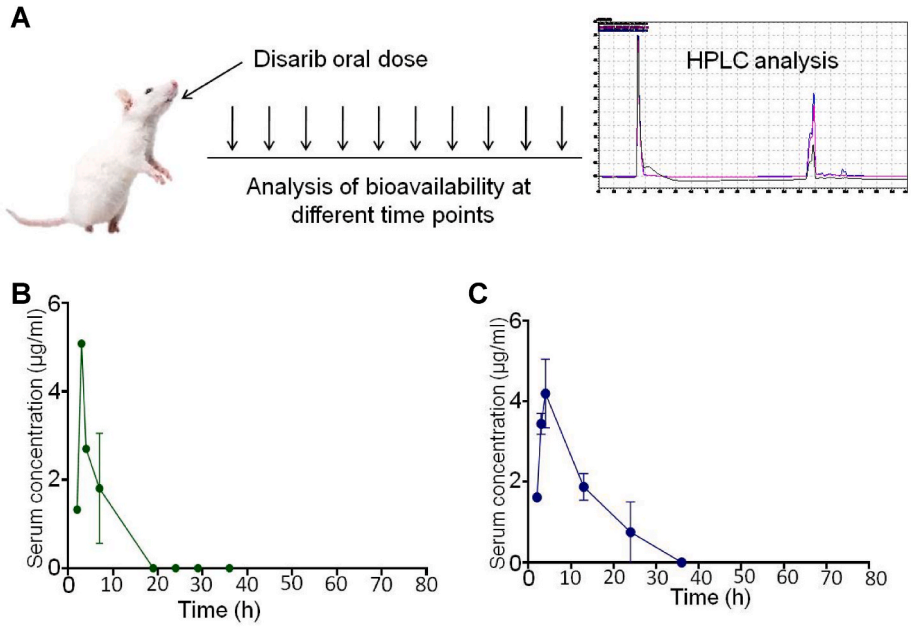

Fig. 7. *In vivo* bioavailability of Disarib in mice. A. Schematic representation of the experimental flow of bioavailability of Disarib in mice. B, C. *In vivo* bioavailability analysis of Disarib in the serum of mice at 0.25, 0.50, 1, 2, 4, 6, 8, 10, 12, 24, 48, 72 h after treatment of Disarib Ss (B) and Disarib Ls (C). Each animal was treated with Disarib orally, and serum was collected at specified time points and subjected to HPLC analysis. The area under the curve (AUC) was calculated to obtain bioavailability. HPLC analysis was done at 232 nm wavelength.

shown are derived from a minimum of three independent experiments.

3.10. Cell cycle analysis

MOLT4 cells were treated with increasing concentrations of two batches of Disarib synthesized through Scheme1 and Scheme2 (0.5, 1, 5, 10 µM) for 48 h and subjected to cell cycle analysis, as described before [19,36,47]. Briefly, MOLT4 (25,000 cells ml^{-1}) was seeded in 4 ml media and treated with the two different batches of Disarib, harvested, washed with 1x PBS, and fixed overnight in 70 % ethanol at −20 °C. Fixed samples were treated with RNase A (100 µg ml^{-1}) overnight under shaking conditions at 37 °C. Finally, cells were stained with Propidium Iodide and acquired using a flow cytometer. CytoFLEX flow cytometer, Beckman Coulter (Brea, CA, USA) or BD FACS Verse were used for sample acquisition, while CYTEXPERT and FLUOVIEW software were used for analysis.

3.11. Animals

Swiss albino mice (6–8 weeks old) were purchased from the Central Animal Facility, IISc, Bangalore, and were maintained according to the guidelines of the Animal Ethical Committee. Mice were housed in polypropylene cages and kept in controlled lighting of 12 h light/dark cycle. The animals were provided a standard pellet diet (Altromin, gesundheit für Tiere, Germany) and water ad libitum. Autoclaved corncob was used as bedding material. Maintenance and handling of the animals were according to the Institutional Animal Ethical Committee (IAEC) guidelines. The experimental design and methods followed institutional guidelines. They were approved by the IAEC of the Indian Institute of Science, Bangalore (Ethical committee approval No: CAF/Ethics/744/2020).

3.12. Breast adenocarcinoma tumor model

Ehrlich ascites breast carcinoma (EAC) cells (10×10^5) were injected into the left thigh region of Swiss albino mice and a tumor was induced as described before [13,39,44]. Treatment started once after the tumor was developed. For IP tumor studies, the control group (n = 8), Disarib Ss, (n = 10), and Disarib Ls, (n = 5) were used. Whereas for oral studies, the control group (n = 10), Disarib Ss, (n = 12), and Disarib Ls, (n = 12) were used for the study. The IP-treated group was given 10 mg/kg b. wt of Disarib, a total of 6 doses (every alternate day). For the oral-treated group 50 mg/kg b. wt dose of Disarib, for continuous 14 days was administered to the animals. The tumor size was measured using vernier caliper up to 24 days, and tumor volume was calculated using the formula: $V = 0.5 \times a \times b^2$, where 'a' and 'b' indicate major and minor tumor diameters, respectively [23,44,49].

3.13. Histopathology

Histopathological evaluation through Hematoxylin-Eosin (HE) staining was done by collecting 25-day-old tumor, liver, and kidney tissues from control animals and animals treated with Disarib-Ls through intraperitoneal (10 mg/kg) and oral (50 mg/kg) route. The tissues were fixed in 4 % paraformaldehyde and processed according to previously published protocols [35,45,49]. Processed tissues were embedded in paraffin wax blocks and sliced into 5 µm sections in a rotary microtome (Leica Biosystems, Buffalo Grove, IL, USA). The sections were deparaffinized and stained with standard eosin hematoxylin protocols [38,40,41,44,45,49] before dehydration and mounting. The sections were then photographed by bright field microscopy (Carl Zeiss Axiovision, Oberkochen, Germany).

3.14. Pharmacokinetic analysis of Disarib

In the pharmacokinetics analysis of Disarib, mice (Swiss Albino) were orally administered with 50 mg/kg Disarib. Blood samples were collected at various time points (15 min–72 h) following Disarib treatment [35,38]. The blood was allowed to clot, and serum was separated through centrifugation and deproteinization. Standard calibration curve samples were prepared by spiking 100 μM Disarib in mice. HPLC analysis was conducted using a Shimadzu HPLC system with a C18 column and an acetonitrile:water gradient. Disarib-specific peaks were detected at 232 nm wavelength. Pharmacokinetic parameters were analyzed using LabSolutions software, and data was plotted with GraphPad Prism software. Maximum drug plasma concentration (Cmax), time to reach Cmax, clearance (Cl), and steady-state volume of distribution (Vss) were calculated.

3.15. HPLC analysis

For HPLC analysis, the samples were analyzed using the Shimadzu HPLC system with a C18 analytical column. The mobile phase consisted of a gradient of acetonitrile and water. Disarib-specific peaks were detected at 232 nm wavelength. The injection volume was 20 μl, and the flow rate was 1.2 ml/min. Standard curves were constructed by plotting the peak area against the concentration of Disarib [15,45].

3.16. Statistical analysis

For each experiment, a Student's t-test (two-tailed), using Graph-Pad prism (Version 5.1), was employed to calculate the statistical significance of the results reported. Values with p-value less than 0.05 were considered significant. Values are presented as mean ± SEM. $p < 0.05$ = *, $p < 0.01$ = **, $p < 0.001$ = ***, $p < 0.0001$ = **** were used for representation.

Associated content

Characterization data-NMR spectra, Mass spectra and HPLC analysis (PDF).

Funding

Prof. Sathees C. Raghavan reports financial support was provided by Department of Biotechnology, New Delhi, India. Prof. Sathees C. Raghavan reports financial support was provided by IISc-DBT partnership program. Shivangi Sharma reports financial support was provided by Department of Biotechnology, New Delhi, India. If there are other authors, they declare that they have no known competing financial interests or personal relationships that could have appeared to influence the work reported in this paper.

CRediT authorship contribution statement

Manthra Raveendran: Writing – review & editing, Writing – original draft, Methodology, Data curation. **Shivangi Sharma:** Writing – review & editing, Writing – original draft, Validation, Methodology, Data curation, Conceptualization. **Sanjay Sambhajirao Palimkar:** Methodology. **M. Lakshmana Kumar:** Methodology. **H. Sahana:** Methodology. **Hassan A. Swarup:** Writing – review & editing, Validation, Supervision, Formal analysis. **Sathees C. Raghavan:** Writing – review & editing, Writing – original draft, Visualization, Validation, Supervision, Resources, Project administration, Investigation, Funding acquisition, Formal analysis, Conceptualization.

Declaration of competing interest

The authors declare that they have no known competing financial interests or personal relationships that could have appeared to influence the work reported in this paper.

Data availability

Data will be made available on request.

Acknowledgments

This work was supported by grants from the Glue Grant Department of Biotechnology, New Delhi, India (BT/PR23078/MED/29/1253/2017) and the IISc-DBT partnership program [BT/PR27952-INF/22/212/2018] to SCR. SS is supported by a Junior Research Fellowship (JRF) from DBT, India. We thank the Central Animal Facility for providing animals for the experiments (Ethical committee approval No: CAF/Ethics/744/2020) and the FACS facility of the Department of Biochemistry, Indian Institute of Science (IISc), for cell cycle analysis. We also thank the NMR, LCMS and Microtome facilities at IISc.

Appendix A. Supplementary data

Supplementary data to this article can be found online at https://doi.org/10.1016/j.ejmcr.2024.100157.

References

[1] M. Arkin, Protein-protein interactions and cancer: small molecules going in for the kill, Curr. Opin. Chem. Biol. 9 (3) (2005) 317–324, https://doi.org/10.1016/j.cbpa.2005.03.001.
[2] G. Bajaj, X. Wang, S. Agrawal, M. Gupta, A. Roy, Y. Feng, Model-based population pharmacokinetic analysis of nivolumab in patients with solid tumors, CPT Pharmacometrics Syst. Pharmacol. 6 (1) (2017) 58–66, https://doi.org/10.1002/psp4.12143.
[3] L. Campos, J.P. Rouault, O. Sabido, P. Oriol, N. Roubi, C. Vasselon, E. Archimbaud, J.P. Magaud, D. Guyotat, High expression of bcl-2 protein in acute myeloid leukemia cells is associated with poor response to chemotherapy, Blood 81 (11) (1993) 3091–3096.
[4] S.-L. Chan, M.C. Lee, K.O. Tan, L.-K. Yang, A.S.Y. Lee, H. Flotow, N.Y. Fu, M. S. Butler, D.D. Soejarto, A.D. Buss, V.C. Yu, Identification of chelerythrine as an inhibitor of BclXL function, J. Biol. Chem. 278 (23) (2003) 20453–20456, https://doi.org/10.1074/jbc.C300138200.
[5] S. Cory, J.M. Adams, The Bcl2 family: regulators of the cellular life-or-death switch, Nat. Rev. Cancer 2 (9) (2002) 647–656, https://doi.org/10.1038/nrc883.
[6] G.M. Cragg, S.A. Schepartz, M. Suffness, M.R. Grever, The taxol supply crisis. New NCI policies for handling the large-scale production of novel natural product anticancer and anti-HIV agents, J. Nat. Prod. 56 (10) (1993) 1657–1668, https://doi.org/10.1021/np50100a001.
[7] M.S. Davids, A. Letai, ABT-199: taking dead aim at BCL-2, Cancer Cell 23 (2) (2013) 139–141, https://doi.org/10.1016/j.ccr.2013.01.018.
[8] S. Dhepe, S. Kumar, R. Vinayakumar, S.A. Ramareddy, S.S. Karki, Microwave-assisted synthesis and antimicrobial activity of some imidazo[2,1-b][1,3,4] thiadiazole derivatives, Med. Chem. Res. 21 (8) (2012) 1550–1556, https://doi.org/10.1007/s00044-011-9671-8.
[9] Divyaanka Iyer, Sathees C. Raghavan, Targeted cancer therapy: the role of BCL2 inhibitors, in: first ed., in: J.N. Govil (Ed.), Recent Developments in Biotechnology, vol. 7, Drug Discovery, 2013.
[10] S. Elmore, Apoptosis: a review of programmed cell death, Toxicol. Pathol. 35 (4) (2007) 495–516, https://doi.org/10.1080/01926230701320337.
[11] I.J. Enyedy, Y. Ling, K. Nacro, Y. Tomita, X. Wu, Y. Cao, R. Guo, B. Li, X. Zhu, Y. Huang, Y.-Q. Long, P.P. Roller, D. Yang, S. Wang, Discovery of small-molecule inhibitors of bcl-2 through structure-based computer screening, J. Med. Chem. 44 (25) (2001) 4313–4324, https://doi.org/10.1021/jm010016f.
[12] S. Gapil Tiamas, F. Daressy, A. Abou Samra, J. Bignon, V. Steinmetz, M. Litaudon, C. Fourneau, K. Hoong Leong, A. Ariffin, K. Awang, S. Desrat, F. Roussi, Pro-apoptotic carboxamide analogues of natural fislatifolic acid targeting Mcl-1 and Bcl-2, Bioorg. Med. Chem. Lett 30 (7) (2020) 127003, https://doi.org/10.1016/j.bmcl.2020.127003.
[13] V. Gopalakrishnan, S. Dahal, G. Radha, S. Sharma, S.C. Raghavan, B. Choudhary, Characterization of DNA double-strand break repair pathways in diffuse large B cell lymphoma, Mol. Carcinog. 58 (2) (2019) 219–233, https://doi.org/10.1002/mc.22921.
[14] Y. Gutiérrez-Puente, P. Zapata-Benavides, A.M. Tari, G. López-Berestein, Bcl-2-related antisense therapy, Semin. Oncol. 29 (3 Suppl 11) (2002) 71–76, https://doi.org/10.1053/sonc.2002.34058.
[15] D. Iyer, S.V. Vartak, A. Mishra, G. Goldsmith, S. Kumar, M. Srivastava, M. Hegde, V. Gopalakrishnan, M. Glenn, M. Velusamy, B. Choudhary, N. Kalakonda, S. S. Karki, A. Surolia, S.C. Raghavan, Identification of a novel BCL2-specific inhibitor

that binds predominantly to the BH1 domain, FEBS J. 283 (18) (2016) 3408–3437, https://doi.org/10.1111/febs.13815.
[16] K. Afsari, C.M. Eastman, A comparison of construction classification systems used for classifying building product models, in: 52nd ASC Annual International Conference Proceedings, vol. 10, 2016, p. 2016.
[17] K. Lundquist, Proton (1H) NMR spectroscopy, in: Methods in Lignin Chemistry, 1992.
[18] S.S. Karki, K. Panjamurthy, S. Kumar, M. Nambiar, S.A. Ramareddy, K. K. Chiruvella, S.C. Raghavan, Synthesis and biological evaluation of novel 2-aralkyl-5-substituted-6-(4'-fluorophenyl)-imidazo[2,1-b][1,3,4]thiadiazole derivatives as potent anticancer agents, Eur. J. Med. Chem. 46 (6) (2011) 2109–2116, https://doi.org/10.1016/j.ejmech.2011.02.064.
[19] C.V. Kavitha, M. Nambiar, P.B. Narayanaswamy, E. Thomas, U. Rathore, C. S. Ananda Kumar, B. Choudhary, K.S. Rangappa, S.C. Raghavan, Propyl-2-(8-(3,4-difluorobenzyl)-2',5'-dioxo-8-azaspiro[bicyclo[3.2.1] octane-3,4'-imidazolidine]-1'-yl) acetate induces apoptosis in human leukemia cells through mitochondrial pathway following cell cycle arrest, PLoS One 8 (7) (2013) e69103, https://doi.org/10.1371/journal.pone.0069103.
[20] V. Kirkin, S. Joos, M. Zörnig, The role of Bcl-2 family members in tumorigenesis, Biochim. Biophys. Acta Mol. Cell Res. 1644 (2–3) (2004) 229–249, https://doi.org/10.1016/j.bbamcr.2003.08.009.
[21] M. Konopleva, A.M. Tari, Z. Estrov, D. Harris, Z. Xie, S. Zhao, G. López-Berestein, M. Andreeff, Liposomal Bcl-2 antisense oligonucleotides enhance proliferation, sensitize acute myeloid leukemia to cytosine-arabinoside, and induce apoptosis independent of other antiapoptotic proteins, Blood 95 (12) (2000) 3929–3938.
[22] S. Kumar, V. Gopalakrishnan, M. Hegde, V. Rana, S.S. Dhepe, S.A. Ramareddy, A. Leoni, A. Locatelli, R. Morigi, M. Rambaldi, M. Srivastava, S.C. Raghavan, S. S. Karki, Synthesis and antiproliferative activity of imidazo[2,1-b][1,3,4] thiadiazole derivatives, Bioorg. Med. Chem. Lett 24 (19) (2014) 4682–4688, https://doi.org/10.1016/j.bmcl.2014.08.032.
[23] R. Kumari, U. Roy, S. Desai, N.M. Nilavar, A. Van Nieuwenhuijze, A. Paranjape, G. Radha, P. Bawa, M. Srivastava, M. Nambiar, K.N. Balaji, A. Liston, B. Choudhary, S.C. Raghavan, MicroRNA miR-29c regulates RAG1 expression and modulates V(D)J recombination during B cell development, Cell Rep. 36 (2) (2021) 109390, https://doi.org/10.1016/j.celrep.2021.109390.
[24] Y. Lin, J. Fukuchi, R.A. Hiipakka, J.M. Kokontis, J. Xiang, Up-regulation of Bcl-2 is required for the progression of prostate cancer cells from an androgen-dependent to an androgen-independent growth stage, Cell Res. 17 (6) (2007) 531–536, https://doi.org/10.1038/cr.2007.12.
[25] Q. Liu, H.-G. Wang, Anti-cancer drug discovery and development: bcl-2 family small molecule inhibitors, Commun. Integr. Biol. 5 (6) (2012) 557–565, https://doi.org/10.4161/cib.21554.
[26] M.C. Maiuri, G. Le Toumelin, A. Criollo, J.C. Rain, F. Gautier, P. Juin, E. Tasdemir, G. Pierron, K. Troulinaki, N. Tavernarakis, J.A. Hickman, O. Geneste, G. Kroemer, Functional and physical interaction between Bcl-X(L) and a BH3-like domain in Beclin-1, EMBO J. 26 (10) (2007) 2527–2539, https://doi.org/10.1038/sj.emboj.7601689.
[27] T. Oltersdorf, S.W. Elmore, A.R. Shoemaker, R.C. Armstrong, D.J. Augeri, B. A. Belli, M. Bruncko, T.L. Deckwerth, J. Dinges, P.J. Hajduk, M.K. Joseph, S. Kitada, S.J. Korsmeyer, A.R. Kunzer, A. Letai, C. Li, M.J. Mitten, D. G. Nettesheim, S. Ng, S.H. Rosenberg, An inhibitor of Bcl-2 family proteins induces regression of solid tumours, Nature 435 (7042) (2005) 677–681, https://doi.org/10.1038/nature03579.
[28] F. Ong, K. Kim, M.Y. Konopleva, Venetoclax resistance: mechanistic insights and future strategies, Cancer Drug Resistance (Alhambra, Calif.) 5 (2) (2022) 380–400, https://doi.org/10.20517/cdr.2021.125.
[29] G.F. Perini, G.N. Ribeiro, J.V. Pinto Neto, L.T. Campos, N. Hamerschlak, BCL-2 as therapeutic target for hematological malignancies, J. Hematol. Oncol. 11 (1) (2018) 65, https://doi.org/10.1186/s13045-018-0608-2.
[30] G. Radha, S.C. Raghavan, BCL2: a promising cancer therapeutic target, Biochim. Biophys. Acta Rev. Canc 1868 (1) (2017) 309–314, https://doi.org/10.1016/j.bbcan.2017.06.004.
[31] U. Ray, V.K. Gopinatha, S. Sharma, L. Goyary, B. Choudhary, K. Mantelingu, K. S. Rangappa, S.C. Raghavan, Identification and characterization of mercaptopyrimidine-based small molecules as inhibitors of nonhomologous DNA end joining, FEBS J. 290 (3) (2023) 796–820, https://doi.org/10.1111/febs.16615.
[32] P.J. Real, Y. Cao, R. Wang, Z. Nikolovska-Coleska, J. Sanz-Ortiz, S. Wang, J. L. Fernandez-Luna, Breast cancer cells can evade apoptosis-mediated selective killing by a novel small molecule inhibitor of bcl-2, Cancer Res. 64 (21) (2004), https://doi.org/10.1158/0008-5472.CAN-04-0945, 7947 LP – 7953.
[33] J.C. Reed, Bcl-2 family proteins: regulators of apoptosis and chemoresistance in hematologic malignancies, Semin. Hematol. 34 (4 Suppl 5) (1997) 9–19.
[34] A.W. Roberts, Therapeutic development and current uses of BCL-2 inhibition, Hematology 2020 (1) (2020) 1–9, https://doi.org/10.1182/hematology.2020000154.
[35] R. Sebastian, S.C. Raghavan, Exposure to Endosulfan can result in male infertility due to testicular atrophy and reduced sperm count, Cell Death Discovery 1 (2015) 15020, https://doi.org/10.1038/cddiscovery.2015.20.
[36] M.S. Shahabuddin, M. Gopal, S.C. Raghavan, Intercalating, cytotoxic, antitumour activity of 8-chloro and 4-morpholinopyrimido [4′,5′:4,5]thieno(2,3-b)quinolines, J. Photochem. Photobiol. B Biol. 94 (1) (2009) 13–19, https://doi.org/10.1016/j.jphotobiol.2008.09.001.
[37] S. Shangary, D.E. Johnson, Peptides derived from BH3 domains of bcl-2 family members: a comparative analysis of inhibition of bcl-2, bcl-x $_L$ and bax oligomerization, induction of cytochrome *c* release, and activation of cell death, Biochemistry 41 (30) (2002) 9485–9495, https://doi.org/10.1021/bi025605h.
[38] A. Sharma, A. Kaninathan, S. Dahal, S. Kumari, B. Choudhary, S.C. Raghavan, Exposure to endosulfan can cause long term effects on general biology, including the reproductive system of mice, Front. Genet. 13 (2022), https://doi.org/10.3389/fgene.2022.1047746.
[39] S. Sharma, K. Panjamurthy, B. Choudhary, M. Srivastava, M. Shahabuddin, R. Giri, G.M. Advirao, S.C. Raghavan, A novel DNA intercalator, 8-methoxy pyrimido [4',5':4,5]thieno (2,3-b)quinoline-4(3H)-one induces apoptosis in cancer cells, inhibits the tumor progression and enhances lifespan in mice with tumor, Mol. Carcinog. 52 (6) (2013) 413–425, https://doi.org/10.1002/mc.21867.
[40] S. Sharma, K.K. Varsha, S. Kumari, V. Gopalakrishnan, A.E. Jose, B. Choudhary, K. Mantelingu, S.C. Raghavan, Acute toxicity analysis of Disarib, an inhibitor of BCL2, Sci. Rep. 10 (1) (2020) 15188, https://doi.org/10.1038/s41598-020-72058-8.
[41] S. Sharma, K.K. Varsha, U. Ray, H. Siddiqua, A.E. Jose, S. Muninarasimaiah, S. C. Raghavan, B. Choudhary, Acute toxicity analysis of an inhibitor of BCL2, Disarib, in rats, Sci. Rep. 11 (1) (2021) 9982, https://doi.org/10.1038/s41598-021-89387-x.
[42] R. Singh, A. Letai, K. Sarosiek, Regulation of apoptosis in health and disease: the balancing act of BCL-2 family proteins, Nat. Rev. Mol. Cell Biol. 20 (3) (2019) 175–193, https://doi.org/10.1038/s41580-018-0089-8.
[43] A.J. Souers, J.D. Leverson, E.R. Boghaert, S.L. Ackler, N.D. Catron, J. Chen, B. D. Dayton, H. Ding, S.H. Enschede, W.J. Fairbrother, D.C.S. Huang, S.G. Hymowitz, S. Jin, S.L. Khaw, P.J. Kovar, L.T. Lam, J. Lee, H.L. Maecker, K.C. Marsh, S. W. Elmore, ABT-199, a potent and selective BCL-2 inhibitor, achieves antitumor activity while sparing platelets, Nat. Med. 19 (2) (2013) 202–208, https://doi.org/10.1038/nm.3048.
[44] M. Srivastava, M. Hegde, K.K. Chiruvella, J. Koroth, S. Bhattacharya, B. Choudhary, S.C. Raghavan, Sapodilla plum (Achras sapota) induces apoptosis in cancer cell lines and inhibits tumor progression in mice, Sci. Rep. 4 (2014) 6147, https://doi.org/10.1038/srep06147.
[45] M. Srivastava, M. Nambiar, S. Sharma, S.S. Karki, G. Goldsmith, M. Hegde, S. Kumar, M. Pandey, R.K. Singh, P. Ray, R. Natarajan, M. Kelkar, A. De, B. Choudhary, S.C. Raghavan, An inhibitor of nonhomologous end-joining abrogates double-strand break repair and impedes cancer progression, Cell 151 (7) (2012) 1474–1487, https://doi.org/10.1016/j.cell.2012.11.054.
[46] K.E. Tagscherer, A. Fassl, B. Campos, M. Farhadi, A. Kraemer, B.C. Böck, S. Macher-Goeppinger, B. Radlwimmer, O.D. Wiestler, C. Herold-Mende, W. Roth, Apoptosis-based treatment of glioblastomas with ABT-737, a novel small molecule inhibitor of Bcl-2 family proteins, Oncogene 27 (52) (2008) 6646–6656, https://doi.org/10.1038/onc.2008.259.
[47] E. Thomas, V. Gopalakrishnan, R.R. Somasagara, B. Choudhary, S.C. Raghavan, Extract of vernonia condensata, inhibits tumor progression and improves survival of tumor-allograft bearing mouse, Sci. Rep. 6 (2016) 23255, https://doi.org/10.1038/srep23255.
[48] L.F. Tietze, Domino reactions in organic synthesis, Chem. Rev. 96 (1) (1996), https://doi.org/10.1021/cr950027e.
[49] S.V. Vartak, M. Hegde, D. Iyer, S. Gaikwad, V. Gopalakrishnan, M. Srivastava, S. S. Karki, B. Choudhary, P. Ray, T.R. Santhoshkumar, S.C. Raghavan, A novel inhibitor of BCL2, Disarib abrogates tumor growth while sparing platelets, by activating intrinsic pathway of apoptosis, Biochem. Pharmacol. 122 (2016) 10–22, https://doi.org/10.1016/j.bcp.2016.09.028.
[50] S.V. Vartak, D. Iyer, T.R. Santhoshkumar, S. Sharma, A. Mishra, G. Goldsmith, M. Srivastava, S. Srivastava, S.S. Karki, A. Surolia, B. Choudhary, S.C. Raghavan, Novel BCL2 inhibitor, Disarib induces apoptosis by disruption of BCL2-BAK interaction, Biochem. Pharmacol. 131 (2017) 16–28, https://doi.org/10.1016/j.bcp.2017.02.015.
[51] S.V. Vartak, H.A. Swarup, V. Gopalakrishnan, V.K. Gopinatha, V. Ropars, M. Nambiar, F. John, S.K.S. Kothanahally, R. Kumari, N. Kumari, U. Ray, G. Radha, D. Dinesh, M. Pandey, H. Ananda, S.S. Karki, M. Srivastava, J.B. Charbonnier, B. Choudhary, S.C. Raghavan, Autocyclized and oxidized forms of <scp>SCR</scp> 7 induce cancer cell death by inhibiting nonhomologous <scp>DNA</scp> end joining in a Ligase <scp>IV</scp> dependent manner, FEBS J. 285 (21) (2018) 3959–3976, https://doi.org/10.1111/febs.14661.
[52] M. Vogler, D. Dinsdale, M.J.S. Dyer, G.M. Cohen, Bcl-2 inhibitors: small molecules with a big impact on cancer therapy, Cell Death Differ. 16 (3) (2009) 360–367, https://doi.org/10.1038/cdd.2008.137.
[53] J.L. Wang, Z.J. Zhang, S. Choksi, S. Shan, Z. Lu, C.M. Croce, E.S. Alnemri, R. Korngold, Z. Huang, Cell permeable Bcl-2 binding peptides: a chemical approach to apoptosis induction in tumor cells, Cancer Res. 60 (6) (2000) 1498–1502.
[54] M. Wang, H. Wang, H. Zheng, D. Uhrin, R.J. Dewhurst, R. Roehe, Comparison of HPLC and NMR for quantification of the main volatile fatty acids in rumen digesta, Sci. Rep. 11 (1) (2021) 24337, https://doi.org/10.1038/s41598-021-03553-9.
[55] Z. Wang, A.S. Azmi, A. Ahmad, S. Banerjee, S. Wang, F.H. Sarkar, R. M. Mohammad, TW-37, a small-molecule inhibitor of bcl-2, inhibits cell growth and induces apoptosis in pancreatic cancer: involvement of notch-1 signaling pathway, Cancer Res. 69 (7) (2009) 2757–2765, https://doi.org/10.1158/0008-5472.CAN-08-3060.